APPLIED ECOLOGY

Effects of a deep-sea mining experiment on seafloor microbial communities and functions after 26 years

T. R. Vonnahme[1]*[†], M. Molari[1], F. Janssen[1,2], F. Wenzhöfer[1,2], M. Haeckel[3], J. Titschack[4,5], A. Boetius[1,2,4]

Future supplies of rare minerals for global industries with high-tech products may depend on deep-sea mining. However, environmental standards for seafloor integrity and recovery from environmental impacts are missing. We revisited the only midsize deep-sea disturbance and recolonization experiment carried out in 1989 in the Peru Basin nodule field to compare habitat integrity, remineralization rates, and carbon flow with undisturbed sites. Plough tracks were still visible, indicating sites where sediment was either removed or compacted. Locally, microbial activity was reduced up to fourfold in the affected areas. Microbial cell numbers were reduced by ~50% in fresh "tracks" and by <30% in the old tracks. Growth estimates suggest that microbially mediated biogeochemical functions need over 50 years to return to undisturbed levels. This study contributes to developing environmental standards for deep-sea mining while addressing limits to maintaining and recovering ecological integrity during large-scale nodule mining.

INTRODUCTION

Polymetallic nodules cover large areas of the Pacific and Indian Ocean and have high concentrations of valuable metals, such as copper, nickel, and cobalt (1). Exploiting these and other deep-sea metal resources is discussed as an alternative to terrestrial mining to reduce the environmental impacts on vulnerable land ecosystems while accommodating shifting political dependencies (1, 2). However, the deep-sea ecosystem and effects of anthropogenic disturbances on these ecosystems and their inhabitants are poorly understood, thereby limiting impact and recovery assessments (2, 3), as well as establishing management rules for the avoidance of "serious harm" to the ecosystem (4). Only a few benthic impact experiments have taken place in the deep sea (5), among them the unique DISturbance and reCOLonization experiment (DISCOL). The DISCOL impact study was started in 1989 in the Peru Basin of the South Pacific at 7°S and 88.5°W. Recovery was previously assessed in 1989, 1992, and 1996 (3) until this study in 2015. During DISCOL, the impact of deep-sea mining on the benthic ecosystem was simulated by ploughing the ~4150-m-deep seafloor repeatedly with a plough harrow in an area of 11 km² (3). The current study revisited the DISCOL experimental area (DEA) in 2015, 26 years after the impact was set, as part of the European Joint Programming Initiative (JPI) Oceans project MiningImpact. The main purpose was to assess long-term environmental impacts on benthic communities, their activities, and their sedimentary environment.

Most of the previous studies on the potential impact of deep-sea mining of manganese nodules investigated the effects of disturbances on the distribution, composition, and activities of deep-sea fauna. However, only very few studies looked at biogeochemical functions, which were limited to fluxes of different elements and nutrients (3, 6, 7). It was postulated that the removal of nodules would lead to a loss of seafloor integrity with the main impact being the removal of the biologically active surface layer; however, evidence from spatially replicated sampling was missing until now (7–10). In the Peru Basin, the reactive surface layer is visible as a brown oxygenated sediment layer with high manganese oxide (MnO_2) concentrations (11) characterized by relatively high biological activities, such as bioturbation and aerobic microbial remineralization (8, 9). It was hypothesized that the removal of this layer could cause a substantial decrease in the labile organic matter pool originating from the deposition of particles exported from the productive ocean surface layer, representing the main food source to the benthos (8). However, previous studies were not able to assess changes in microbial communities, activities, and in situ respiration rates simultaneously, leaving this hypothesis untested.

The aim of the present study was to quantify the potential long-term impacts of deep-sea mining–related disturbances on seafloor integrity, with a focus on the long-term changes of microbial communities, their functions, and their potential for recovery from seafloor disturbance and nodule removal. In the 26-year-old plough tracks, as well as in fresh tracks, the effects on organic matter remineralization and microbial biomass production were investigated using a broad spectrum of state-of-the-art methods in microbiology and biogeochemistry. Three reference sites outside the DEA, three disturbance sites within the DEA, and a fresh, 5-week-old track created with an epibenthic sledge (EBS; a towed instrument to sample organisms at the seafloor) were sampled and compared. The main hypotheses tested were as follows:

1) Damage of seafloor integrity by nodule removal and sediment compaction is long-lasting due to low sedimentation rates, low current speeds, and low bioturbation activities.

2) Microbial cell abundance, remineralization, and secondary production rates are sensitive variables to assess seafloor disturbance and recovery.

3) Seafloor, which has lost the productive surface layer, differs in microbial community structure and function from undisturbed seafloor (short term and long term).

[1]Max-Planck Institute for Marine Microbiology, Bremen, Germany. [2]HGF MPG Group for Deep Sea Ecology and Technology, Alfred Wegener Institute for Polar and Marine Research in the Helmholtz Association, Bremerhaven, Germany. [3]GEOMAR Helmholtz Center for Ocean Research Kiel, Kiel, Germany. [4]MARUM–Center for Marine Environmental Sciences, University of Bremen, Bremen, Germany. [5]Senckenberg am Meer, Marine Research Department, Wilhelmshaven, Germany.
*Corresponding author. Email: tobias.vonnahme@uit.no
†Present address: Department of Arctic and Marine Biology, UiT, the Arctic University of Norway, Tromsø, Norway.

RESULTS

Seafloor integrity based on physical and biogeochemical properties

The plough tracks were clearly visible, and their exact position was determined by georeferenced side-scan sonar seafloor backscatter mapping with the Autonomous Underwater Vehicle Abyss (12). Video footage collected with the remotely operated vehicle (ROV) showed relatively similar manganese nodule abundances in all reference stations (ca. 1 to 5/m^2) (13) and in the DEA outside the tracks (see Fig. 1C) (13). The 26-year-old plough tracks in the DEA ("DEA plough track") were clearly devoid of nodules (see Fig. 1A). These were ploughed under or pushed to the sides of the tracks. Clearly distinguishable structures ("microhabitats") included ridge and furrow structures and whitish sediment patches where subsurface sediments were exposed ("subsurface patches"). The whitish color of the subsurface layers is attributed to the color of Fe(II) in the clay minerals and the high calcium carbonate content (9). Outside the plough tracks, the DEA seafloor was smooth and relatively homogenous ("outside") with regard to roughness from nodule coverage. In some areas, nodules appeared somewhat dusted with sediments. The fresh track produced with an EBS during the expedition was visible as a ca. 15- to 20-cm-deep trench, often showing the whitish subsurface sediments exposed (Fig. 1B). The surface of this track ("EBS track") appeared relatively flat with lumps of sediment piled up at the sides ("EBS pile"; see Fig. 1B). The sampling design of this study is further detailed in Materials and Methods and fig. S1.

Computer tomography (CT) scans of sediment cores obtained from the reference stations showed a rather homogenous 10- to 15-cm-deep surface layer that had a lower x-ray attenuation, a proxy for the sediment density (in the following referred to as "density"), compared with deeper layers (Fig. 2B). This agrees with porosity measurements, which had opposite trends to density and showed generally higher values (i.e., higher water content) in the surface layer of all microhabitats (Fig. 3B). Below this layer, densities increased, and porosity decreased with depth (figs. S2 and S3). In the subsurface sediments [14 to 16 cm below the seafloor (bsf)] and where the subsurface was exposed, i.e., in the EBS track or in the whitish patches in the plough tracks, the density was higher and the porosity lower than at the reference stations (Fig. 3B). Surface layer densities outside the plough tracks in the DEA were similar to those of the reference stations. Despite pronounced lateral variability, generally higher values (i.e., higher water content) were found in the surface layer of all microhabitats (Fig. 3B). CT scans revealed numerous bioturbation channels that extended from the sediment surface down to about 15 cm bsf and the presence of buried nodules in some of the cores (Fig. 2A). Bioturbation channels in the surface of the DEA cores from both in and outside the plough tracks were fewer than in the reference cores and, to a larger part, were disconnected from deeper channels that did not extend to the seafloor, indicating a formation before the disturbance. Sediment cores in the tracks seemed to have even less bioturbation channels. Only in the plough furrows, a few bioturbation channels reached the seafloor. The low-density surface layer was thinner than at the reference stations, especially in the plough ridges, but also in the furrows. In both the subsurface patches exposed by ploughing 26 years ago and in the fresh EBS track, the surface layer was absent. A less dense layer was visible in deeper layers of the subsurface patch sites that seemed to be disconnected from sediment structures above and below. Cracks were visible in some ridge cores, in the EBS track, and in the EBS pile. The EBS track core showed sediment clods
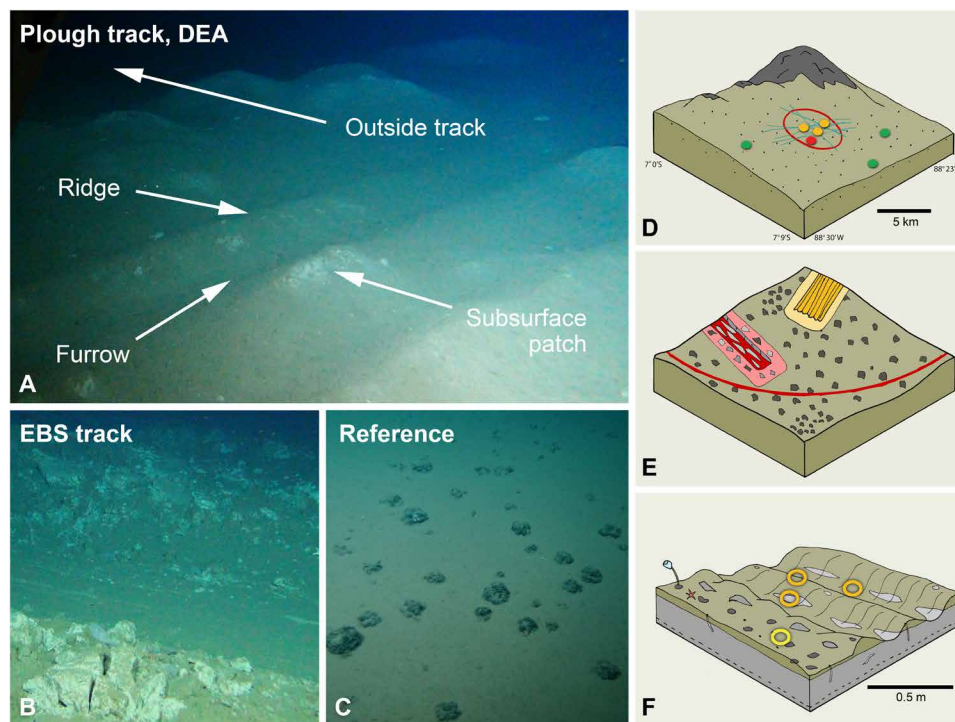

Fig. 1. Photographs of the sampling sites. (**A**) DEA plough track (photo credit: ROV Kiel 6000 Team, GEOMAR), showing the different microhabitat samples; (**B**) EBS track [photo credit: Ocean Floor Observation System (OFOS), Alfred-Wegener Institute (AWI)]; and (**C**) the Reference (photo credit: ROV Kiel 6000 Team, GEOMAR). (**D** to **F**) Schematic representation of the sampling design (A) and different microhabitats observed (photo credit: Autun Purser).
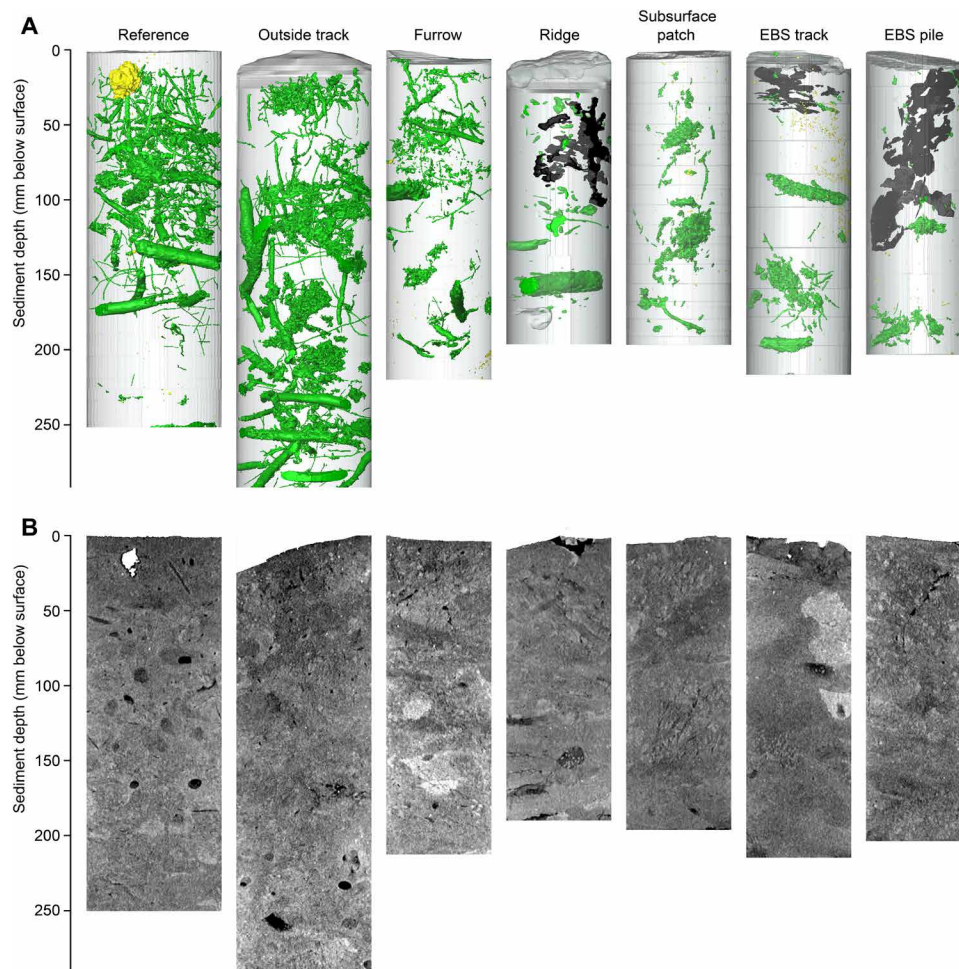
Fig. 2. CT scan results of representative sediment cores from different microhabitats. (y axis ± 2 cm) showing (**A**) bioturbation channels (green), manganese nodules (yellow), and cracks (black/dark-gray), and (**B**) middle layer of the CT showing the sediment densities (x-ray attenuation) with higher densities appearing lighter.

on top and an old, strongly eroded manganese nodule close to the surface.

The depth of the brown manganese oxide–rich layer ("brown layer"), as observed visually in the freshly collected cores, corresponded to the less dense surface layer in the CT scans. This oxygenated layer, where most of the biogeochemical activity was expected, was the primary focus of this study, as well as the top centimeter layer ("top layer"), where labile organic matter and benthic biota abundances were typically highest (8). The brown layer was thickest at the reference stations (extending ca. 10 to 15 cm bsf) and outside the tracks (Fig. 3A). Compared with the reference stations, the brown layer was significantly shallower in the plough furrows and ridges (ca. 5 cm bsf; Kruskal-Wallis test, $P < 0.05$; table S1), and absent where patches of subsurface sediments were exposed by deep ploughing in 1989 or in the fresh EBS track (Fig. 3A). The surface sediment layer inside the fresh EBS tracks was completely removed to a sediment depth of ca. 15 to 20 cm, as indicated by the ROV pictures (Fig. 1), CT scans (Fig. 2), and brown layer depth (Fig. 3A). At the reference stations, oxygen penetration corresponded to the brown layer depth (ca. 10 cm bsf) (Fig. 3A). Oxygen penetrated deeper in furrows, subsurface patches, and outside tracks (12 to 14 cm bsf; Fig. 3A) than in the reference stations. Oxygen penetration was shallower in the EBS track and the ridges (Fig. 3A).

We carried out biogeochemical analyses to analyze the effects of ploughing on carbon and nitrogen availability and its distribution. For the following sections, values for all stations and microhabitats are described for the top layer (0 to 1 cm) of the sediment unless specified differently. Total inorganic carbon (TIC) concentrations (Fig. 3C) and total alkalinity (TA) (Table 1) were significantly increasing with sediment depth and significantly lower in the brown layers of all microhabitats in the DEA (Fig. 3C). The highest values of TA and TIC in the top layer were found in the EBS track and subsurface patches, followed by the other microhabitats in the DEA (Table 1 and Fig. 3C), congruent with the removal of the bioactive layer. Porewater concentrations of reduced iron were close to detection limit and showed no depth trend (Table 1 and Fig. 3C). Nitrate and ammonium had high concentrations throughout the sediment cores with small differences between the microhabitats. Nitrite had a distinctive peak close to the surface, which was narrower in the subsurface patches and virtually absent in the EBS track (Fig. 3D).

Microbial cell abundances and biological functions
Compared with the reference sites, biological processes in the top centimeter were significantly reduced in the fresh EBS track. In addition, the 26-year-exposed subsurface patches and ridges of the plough tracks showed reduced biological activity (Fig. 4), including
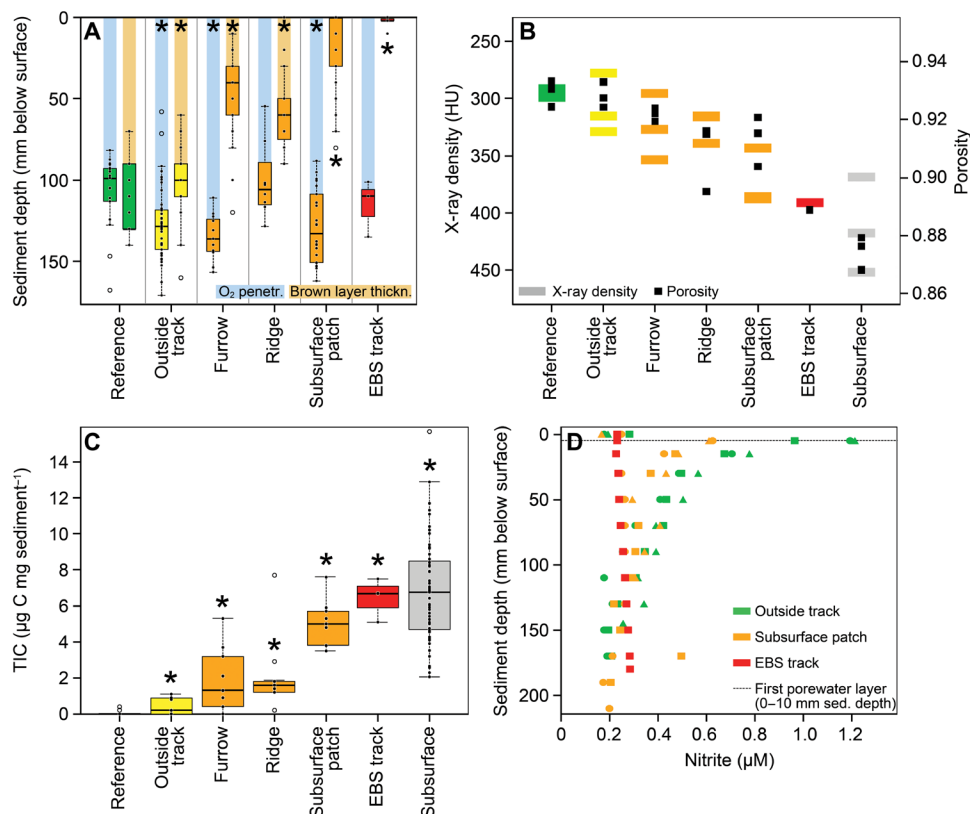
Fig. 3. Sediment characteristics of the different microhabitats. Boxplots show the median (horizontal line), interquartile ranges (box limits), range (whiskers), outliers (circles), and individual data points (dots). Significant differences from the reference are indicated with an asterisk (test statistics in table S1). The colors represent the different sampling sites: reference station (green); outside the DEA tracks (yellow); DEA track furrows, ridges, and subsurface patches (orange); fresh EBS track (red); and subsurface, i.e., at 14 to 16 cm bsf (gray). (**A**) Oxygen penetration depth (blue bar) and MnO_2^--rich brown layer depth (brown bar). (**B**) Average x-ray density (■) and porosity at the top centimeter (■) ($n = 3$). (**C**) TIC concentrations of the top centimeter ($n = 3$ for EBS; others $n = 9$). (**D**) Nitrite (NO_2^-) profiles of the cores outside the tracks, the subsurface patches, and the EBS track ($n = 3$).

microbial dark CO_2 fixation (DCF) rates (Fig. 4A). Respiration rates, estimated as diffusive [diffusive oxygen uptake (DOU); Fig. 4B] and total oxygen uptake (TOU) rates [interquartile ranges (IQ) 0.5 to 1 mmol C m^{-2} day^{-1}; fig. S4] were generally reduced in all DISCOL microhabitats (IQ, 0.5 to 0.9 mmol C m^{-2} day^{-1}) compared with the reference sites (IQ, 0.6 to 1.1 mmol C m^{-2} day^{-1}). Differences were only significant in case of the better replicated DOU measurements. All measured extracellular enzymatic activities relevant in the hydrolysis of large organic molecules (e.g., beta-glucosidase in Fig. 4C; see also fig. S4), with the exception of aminopeptidase (fig. S7), were the most reduced in the EBS track, followed by the subsurface patches and ridges. Aminopeptidase was only lower in the subsurface patch (fig. S7).

Total cell counts were approximately 3×10^8 cells ml^{-1} of wet sediment in the top layer of the reference stations and outside the track (Fig. 4D). Organic matter concentrations in the top layer were approximately 9 μg total organic carbon (TOC) mg^{-1} of dry sediment and 0.09 μg chlorophyll a (Chla) ml^{-1} (Fig. 4E). Microbial abundances and Chla concentrations decreased with sediment depth by a factor of 3 until 14 to 16 cm bsf (Fig. 4D), while TOC decreased by only 15% (Fig. 4E). In the top centimeter of the EBS track, cell numbers were only half of those found in the top centimeter at the reference stations (Fig. 4D), while organic matter concentrations remained at a similar level compared with the reference (Fig. 4E). In the top centimeter of the subsurface patches, cell

numbers were reduced by 30% (Fig. 4D) and Chla approximately by half (Fig. 4E). No significant reduction in cell numbers or organic matter was found in other microhabitats. The patterns prevailed after adjustment for porosity differences (i.e., normalization to dry weight).

Microbial community structure

The bacterial and archaeal community structures of the top centimeter of all microhabitats and the subsurface (14 to 16 cm bsf) were heterogeneous with a large overall spread (Fig. 5A). Nitrifiers constituted a significant part of the microbial community at all sites (approximately 15% relative abundance; fig. S5). No significant differences between the diversity indices inverse Simpson, Shannon Wiener, number of operational taxonomic units (OTUs), or Chao1 have been found between the microhabitats or sampling sites (Kruskal-Wallis test, $P > 0.05$; see fig. S6 and table S2). However, communities from almost all samples were not saturated (fig. S6). We detected relatively large OTU turnovers of 33 to 81% between the samples, showing a considerable microbial biodiversity in the area (table S2). Given the large variability between replicates from the different sites, only the communities of the top centimeter in the EBS track differed significantly from all other samples. The differences between the other microhabitats were not significant. These patterns prevailed after subsampling the communities for different

Table 1. Median values (upper line) and interquartile ranges or min and max (lower line) of measured biogeochemical variables in the top centimeter of each station and at 14 to 16 cm bsf (subsurface). Because of only one replicate for nutrients in the EBS track, no ranges are given. TN, total nitrogen; TOC, total organic carbon; TIC, total inorganic carbon; Chla, chlorophyll a; Phaeo, phaeopigments; NO_2^-, nitrite; NO_3^-, nitrate; NH_4^+, ammonium; Fe^{2+}, ferrous oxide; TA, total alkalinity.

Parameter	Unit	Reference	Outside	Furrow	Ridge	Subsurface patch	EBS track	Subsurface
X-ray density	HU	294	314	326	315	384	390	416
		292–296	296–328	310–339	314–326	363–385	NA	392–433
Porosity		0.93	0.93	0.92	0.91	0.92	0.89	0.88
		0.93–0.93	0.93–0.93	0.92–0.92	0.91–0.92	0.91–0.92	NA	0.87–0.88
TN	μgN mgSed^{-1}	1.3	1.3	1.3	1.2	1.2	0.9	1.1
		1.2–1.4	1.0–1.4	1.2–1.3	1.2–1.3	1.1–1.3	0.9–0.9	0.9–1.1
TOC	μgC mgSed^{-1}	9.1	9.1	8.9	8.2	8.3	9.2	7.7
		9.0–9.4	8.4–9.9	8.5–9.5	7.4–8.3	8.1–8.4	8.9–9.4	7.0–7.8
TIC	μgC mgSed^{-1}	0	0.2	1.3	1.6	5	6.7	5.9
		0–0.4	0–0.9	0.4–3.2	1.2–1.8	3.8–5.7	5.9–7.1	5.8–7.4
Chla	μg ml^{-1}	0.09	0.09	0.07	0.04	0.05	0.07	0.02
		0.07–0.1	0.07–0.09	0.06–0.1	0.04–0.06	0.04–0.06	0.08–0.08	0.02–0.03
Phaeo	μg ml^{-1}	0.23	0.21	0.19	0.13	0.17	0.23	0.1
		0.17–0.25	0.15–0.27	0.16–0.23	0.11–0.14	0.15–0.19	0.22–0.24	0.08–0.11
Chla, relative	%	26	25	27	24	23	25	22
		24–29	23–30	22–28	22–31	22–25	24–27	18–23
NO_2^-	μM	1.3	1.2	1.2	0.8	0.6	0.2	0.2
		1.3–2.1	1.0–1.5	1.1–1.2	0.4–1.0	0.6–2.3	NA	0.2–0.3
NO_3^-	μM	46.2	42	41.9	40.2	42.1	37.9	44.8
		43.8–50.2	40.3–42.6	40.7–42.3	39.3–73.8	39.8–43.0	NA	43.8–72.2
NH_4^+	μM	14.6	12.2	9.5	11.1	8.5	9.8	15.2
		8.9–40.2	6.1–16.4	7.6–12.3	5.7–12.9	7.9–16.5	NA	43.8–72.2
Fe^{2+}	μM	0	0.3	0.2	0	0.2	0.1	0
		0–0.1	0.2–0.3	0.14–0.48	0–0.2	0.2–0.2	NA	0–0.1
TA	meq liter^{-1}	2.1	2.3	2.3	2.2	2.3	2.2	2.4
		2.1–2.2	2.3–2.3	2.3–2.3	2.2–2.2	2.2–2.3	NA	2.4–2.4

groups {i.e., keeping or removing low-abundant OTUs (<1%), keeping differentially abundant OTUs (based on eight differentially abundant OTUs based on ALDEx2, keeping only the most abundant ones), and using different distance matrices (Jaccard on presence-absence data, Euclidean distance), different ordinations [principal components analysis (PCA)], or transformations (i.e., Hellinger, center log ratio)}.

The fresh disturbance in the EBS track was the only microhabitat with unique bacterial OTUs represented by more than one read (i.e., nonsingleton OTUs that appear at only one station) that also showed the highest number of OTU turnover compared with the other microhabitats (see above). OTUs (303), mainly belonging to the Chloroflexi group (about 60% of the unique OTUs), were only found in the EBS track and represented 3.9% of the total sequences. As a general trend, EBS track communities and communities from

the exposed subsurface patches were more similar to the subsurface communities at sediment depths of 14 to 16 cm than to those of the other microhabitats. This was most obvious at DEA west (pyramid-shaped symbols in Fig. 5A), where subsurface patch communities were most similar to subsurface communities and plot relatively closely to EBS track communities. Less similarities to the subsurface communities were found in ridges, while communities in the furrows and the samples outside the track were even more dissimilar to the subsurface and indistinguishable from the reference communities.

Subsurface sediments, subsurface patches, and EBS track were characterized by higher TIC concentrations (Fig. 5B). The high amount of phytopigments in the top layer of the EBS track was likely due to the resettling of a thin layer of suspended sediments. After towing the EBS, larger organic particles with relatively high Chla values settled first. The reference and outside track microhabitats
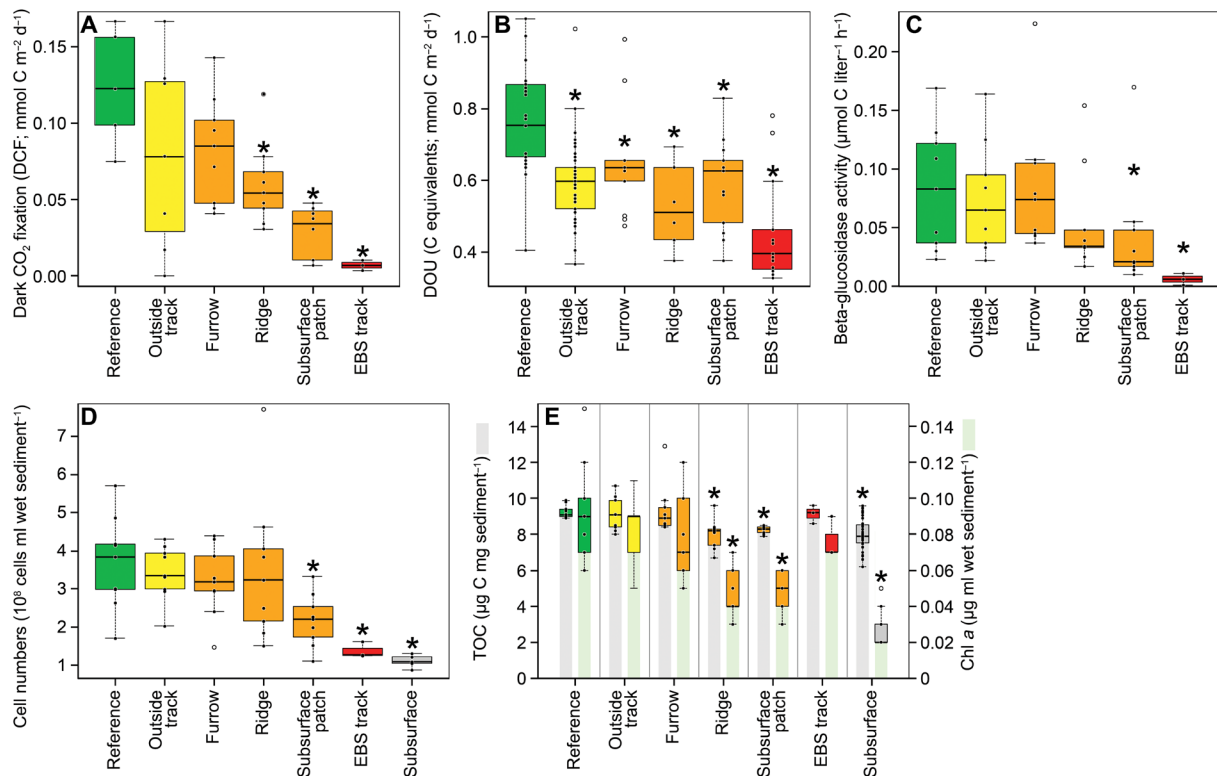
Fig. 4. Biological processes and bacterial and other organic biomass. (**A**) Inorganic carbon uptake into TOC [dark CO_2 fixation (DCF)], (**B**) dissolved oxygen uptake (DOU), and (**C**) potential beta-glucosidase activity as an example of potential extracellular enzyme activities (EEA) measured. Boxplots show the median (horizontal line), interquartile ranges (box limits), range (whiskers), outliers (circles), and individual data points (dots). For the station color code, see Fig. 3. Significant differences from the reference are indicated with an asterisk (test statistics in table S1). (**D**) Cell numbers based on AODC counts. (**E**) TOC (gray bar) and chlorophyll a (green bar) values at the top centimeter. Boxplots show the median (horizontal line), interquartile ranges (box limits), range (whiskers), outliers (circles), and individual data points (dots). Significant differences (Kruskal-Wallis test, $P < 0.05$) from the reference were indicated with an asterisk (test statistics shown in table S1). For the station color code, see Fig. 3.

were characterized by higher TOC, Chla, Phaeo, and total nitrogen (TN). Ridges and furrows have intermediate characteristics (Fig. 5B). Communities in reference east samples were characterized by higher Chla and TOC concentrations and lower TIC, total carbon (TC), Phaeo, and TN concentrations (Fig. 5C).

DISCUSSION

The initial disturbance experiment was designed to simulate physical impacts of deep-sea mining by reworking and dispersing surface sediments and removing manganese nodules from the surface. Accordingly, the plough used caused redistribution of nodules (*14*). Even though the experiment did not plan to accurately simulate nodule removal in industrial processes of deep-sea mining, subsequent studies showed that the removal of nodule in tracks allowed assessing potential mining impacts (*3*). Immediately after ploughing, different disturbances on small spatial scales were observed. Specifically, (i) sediments were resuspended and resettled on and next to the track; (ii) sediment clods were turned upside down, burying surface sediments; and (iii) sediments were redistributed by the ploughshares, creating ridge and furrow structures (*14*). The plough tracks were still present after 26 years according to the autonomous underwater vehicle mosaics (*12*) and ROV surveys (this study). In situ visual observations presented here confirmed that the small-scale morphological features of the disturbance also remained

(Fig. 1). The plough traces (i.e., furrows and ridges) of a few decimeters in height and width were still visible. This can be expected due to low bottom current speeds and low sediment accumulation rates in nodule areas, paucity of large fauna that could cause sediment mixing (*15*, *16*). The main difference to fresh tracks introduced by an EBS were signs of erosion at the ridges of the tracks. Detailed ROV surveys confirmed that manganese nodules were removed by pushing them outside of the tracks or by burying them in sediments. On the basis of physical and biogeochemical data (Figs. 2 and 3), we identified four classes of past disturbances and hypothesize that they represent a gradient of environmental impact from low (i: outside track, some sediment deposition) to severe (iv: removal of active surface layer, exposure of subsurface sediments). Here, we summarize the main impacts observed in terms of seafloor integrity losses (Fig. 6).

Disturbance level i: Outside tracks were marked by some deposition of suspended surface sediments on top of the sediments and nodules adjacent to the plough marks. Some parameters of seafloor integrity and fresh particle supply were very similar to those of the reference stations (phytopigments and porosity), but some differences were discernible in carbon distribution (TIC, TA, and TOC profiles). As in disturbance level ii, recent bioturbation activity was visible.

Disturbance level ii: Ploughing caused depressions (furrows) and subsequent deposition of suspended surface sediments. They show similar disturbances of TIC, TA, vertical TOC distribution,
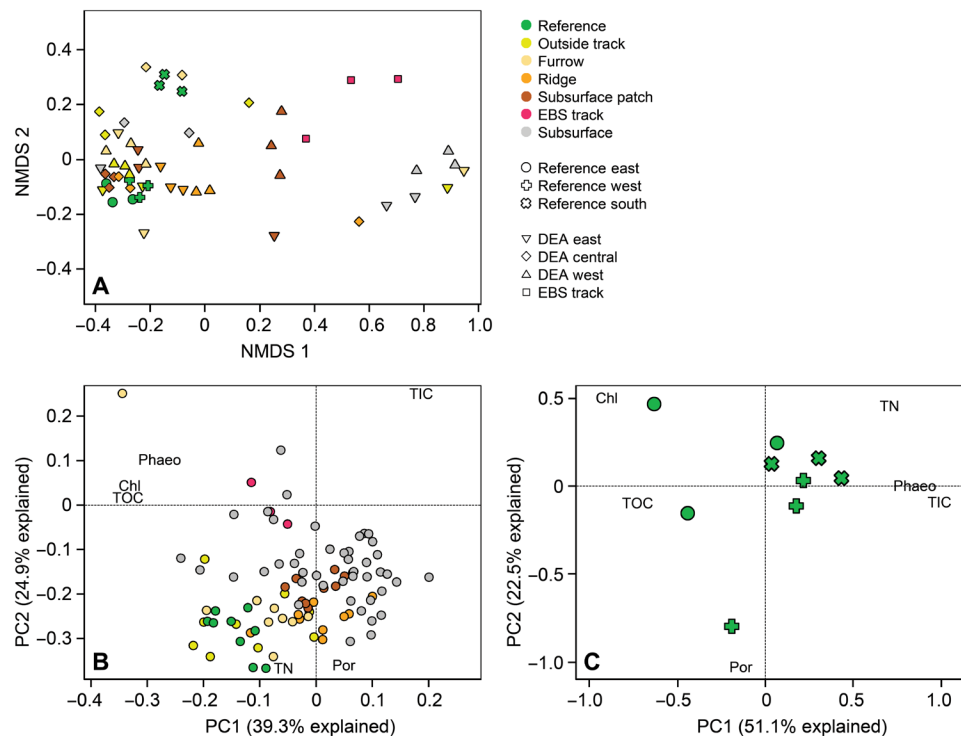
Fig. 5. Biplots showing different community structures and environmental variables. (**A**) NMDS plots, using Bray-Curtis dissimilarities and relative untransformed OTU abundances (stress = 0.06). The colors and symbols indicate the microhabitats and sampling sites, respectively [legend of (A) valid for (A) to (C)]. The locations of the sample points relative to each other indicate their similarity. The closer the points are together, the more similar the samples are based on their community structure. (**B**) Redundancy analyses using different sediment characteristics to separate different sampling sites (sediment characteristics scale 5× reduced). (**C**) Redundancy analyses using different sediment characteristics to separate the different reference stations.

porosity, and oxygen penetration as levels iii and iv, but to a lesser degree. A layer of deposited plume sediment was visible as a thin, homogenous, low-density layer, which lacks a connection to the underlying deep ancient bioturbation channels. This indicates that the furrows created by the plough act as an accumulation spot for fine particles resettling from the suspended sediment plume and/or by net particle trapping during the 26 years since the disturbance experiment (see level iii). CT scans indicate some recent bioturbation activity in the upper sediment layer of the furrows as also observed in disturbance level i and the reference stations (see above).

Disturbance level iii: Plough ridges comprise partially compacted sediments, exposed to erosion and loss of surface sediments. They showed partly deep cracks similar to disturbance level iv. The sediment has characteristics that fall between disturbance level iv (regarding vertical TOC distribution, lower porosity and oxygen penetration, Chla, and lack of bioturbation) and disturbance level ii, with respect to TIC, TA, and TN (see below). Some of the ridges showed signs of surface sediment erosion, marked as ablation of the brown layer.

Disturbance level iv: Where surface sediments were removed by deep ploughing, this led to the loss of the MnO_2-rich brown, oxygenated, and biologically active surface sediments. Such areas showed partly deep cracks and sediment clods on top. The top sediment layer had characteristics similar to the subsurface (14 to 16 cm bsf) with high TIC and TA concentrations and elevated TOC concentrations (Table 1) originating from the last glacial maximum and early Holocene (8, 9, 17). They showed low TN and Chla (Table 1) values, indicating a lower quality and freshness of the

organic matter. The oxygen can penetrate deeper through cracks, but signs of fresh bioturbation are lacking, indicating reduced biological activities and lower remineralization rates.

This study thus confirms our second hypothesis that the impact on seafloor integrity caused significant differences in biogeochemical conditions between the undisturbed reference and the different microhabitats 26 years after the impact. It should be noted that the environmental settings at the three reference stations were rather variable (Fig. 5C), suggesting that for environmental management and impact monitoring, significant replication of sampled areas is needed. For example, sediments at the eastern reference site ("Reference E") have higher Chla and TOC concentrations as compared with Reference W and Reference S, causing a relatively high spatial variability for the baseline. We also assessed vertical variability in sediment cores. For example, subsurface sediments show a somewhat higher TOC content compared with surface sediments because of higher burial efficiency for organic material during the last glacial maximum and Early Holocene (17). Our study suggests that knowledge of the spatial variability of areas dedicated to mining is highly relevant for impact studies and needs to be considered in the planning of baseline analysis including the statistical evaluation of disturbance effects.

In this study, the first data on spatial variability of microbial activities, abundances, and community structure were obtained to test whether these are sensitive variables to assess disturbance and recovery of deep seafloor habitats. These variables had not been investigated during the early disturbance experiment in 1989 (3). Hence, we initiated a small-scale in situ disturbance experiment
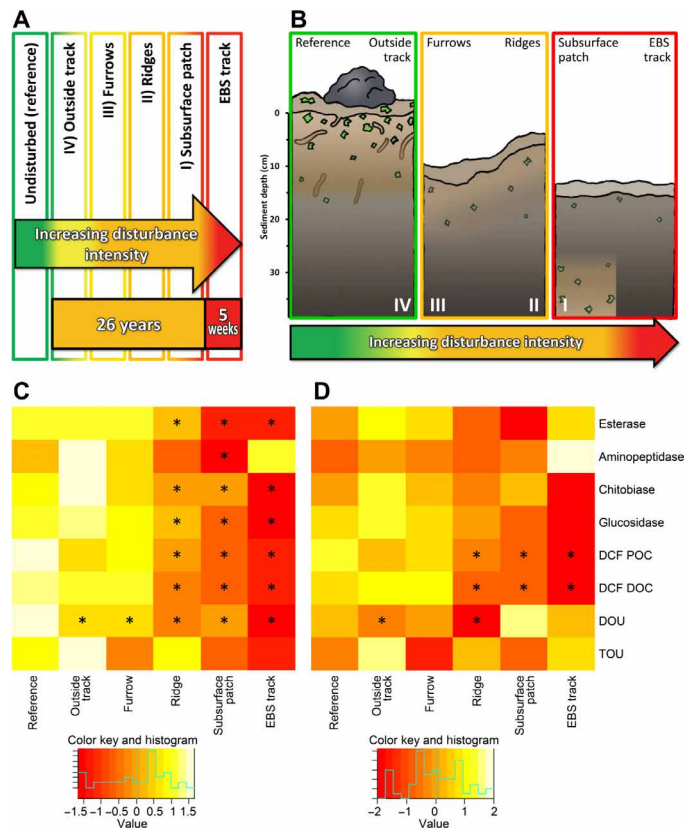
Fig. 6. Synthesis of the observed disturbance gradient. (**A**) Schematic representation of increasing degree of impact from left to right, i.e., green to red color. (**B**) Schematic summary of the differences between the different disturbance levels. (**C** and **D**) Overview of biogeochemical activity per area (C) and per cell numbers (D). Light yellow fields indicate more activity, while orange and red colors represent less activity. The distribution of relatively more and less activity can be seen in the color key histogram on top. The activity is summarized as the median of the z-scaled values (mean = 0, standard deviation = 1). Asterisks indicate significant differences from the reference sites (Kruskal-Wallis, $P < 0.05$; table S1).

carried out with the EBS 5 weeks before sampling (EBS track; Fig. 1B) to compare short- and long-term responses of microbial communities and functions.

A key function of the benthic microbial life dominating the marine seafloor community biomass and diversity is the remineralization of deposited organic matter. Microbial oxygen consumption, measured in situ as DOU, was used as a variable to assess the effects of a loss of seafloor integrity on remineralization rates. This ecological function was significantly reduced in all DEA stations compared with the references, suggesting that sediment blanketing outside the track and sediment removal or reworking in the track were all affecting remineralization rates. Differences along the disturbance gradient in phytopigment content in the surface layer, probably reflecting differences in the suspension and accumulation of detritus particles by the disturbance, did not have an effect on oxygen uptake. This would be the case if organic matter availability would be the only explanation for the reduced oxygen uptake.

We also assessed the difference between predominantly microbial, diffusive benthic oxygen uptake (DOU) and TOU, which includes faunal respiration. DOU and TOU were largely similar, both in terms of absolute values, as well as with regard to the patterns observed

across the different disturbance gradients. This indicates a small contribution of oxygen uptake by fauna and suggests that microorganisms contributed the major part of the observed remineralization rates. While our study showed this in situ in the Pacific, additional sediment studies in other geographical regions found the same. Specifically, Rowe and Deming (18) showed rapid carbon utilization by benthic microbes in deep-sea habitats in the Bay of Biscay and the Demerara Abyssal plain, accounting for up to 30% of the TC consumption. Lochte and Turley (19) found high bacterial and cyanobacterial growth rates on fresh detritus at 4500-m depth under in situ and surface conditions. Kanzog et al. (20), Hoffmann et al. (21), and Boetius et al. (22) found a rapid response of microbial communities and activities to fresh organic matter in the Arctic Ocean.

To address the microbial role in remineralization of organic matter more specifically, we assessed the effect of losses in seafloor integrity on the bulk extracellular hydrolytic enzymatic activity of the microbial community, a rate-limiting step in organic matter degradation, as well as on their dark uptake of CO_2 (DCF), a measure of microbial anabolism. Both methods were applied ex situ, which may lead to different activities compared with in situ activities (23, 24). However, temperature has been identified as a driver of ex situ artifacts (24), an effect we minimized by processing the cores at in situ temperatures. Other effects described by Glud et al. (23) are compression of the sediment matrix, decompression effects of porewater chemistry, and porewater extension, which may be more critical to interpret ex situ oxygen profiles. The effect of pressure in causing ex situ artifacts is quite controversial, as some studies did not find differences between in situ and ex situ growth rates (19) or carbon utilization (18). Our DCF rates match those measured in situ on central Pacific deep-sea sediments (10), suggesting that changes in pressure had a limited effect on our measurements. Overall, ex situ artifacts might be present but appear to play a minor role in our DCF measurements. Extracellular enzymatic activities were also measured ex situ, but the method used only determines potential rates, and our discussion focused on the patterns of the responses to disturbances rather than on total rates.

We compared a fresh disturbance (5 weeks after the EBS tow) with the 26-year-old disturbance by ploughing. On both time scales, the mechanical removal of the bioactive surface layer led to a significant decrease in microbial hydrolytic enzyme activity (especially beta-glucosidase) and anabolic DCF, which concurred with lower cell numbers in the disturbed sediments (Figs. 4 and 6, C and D).

There are indications that a decline in cell-specific metabolism, especially the microbial growth efficiency, could be responsible for some of the negative effects observed. A low microbial growth efficiency is commonly indicated by high respiration rates per cell and low biomass production per cell (25). In the EBS track, plough furrows, and subsurface patches of DEA, biomass production (based on cell-specific DCF) decreased more than cell-specific respiration compared with the reference sites (Fig. 6, C and D, and table S1). To rule out a possible bias from inactive cells counted with the acridine orange direct count (AODC) method, a more conservative approach using overall biomass production based on DCF and overall respiration based on DOU was used (table S1). This resulted in a reduction in growth efficiency by 30 to 45% in the most disturbed microhabitats (table S1).

Extracellular enzymes are subject to positive and negative control mechanisms by substrate supply (26). The generally substrate-induced

beta-glucosidase activities showed a significant decline in response to the disturbance. In contrast, the activity of the enzyme amino-peptidase apparently continuously expressed also by highly energy-limited microbial communities did not decrease in the nutrient-starved subsurface sediments, similar to earlier findings (27). DCF, including turnover into dissolved organic carbon (DOC) (fig. S4), is used as a proxy for overall microbial activity (e.g., anaplerotic reactions and chemosynthesis) (28). The reference values of 0.12 mmol m^{-2} day^{-1} at DISCOL match very well with in situ values measured in the Clarion-Clipperton Zone (CCZ) (0.1 mmol m^{-2} day^{-1}) (10). Anaplerotic reactions may contribute to the DCF (29), but chemolithoautotrophic processes, such as nitrification and metal oxidation (10, 29, 30), are potentially important as well. DCF was also very sensitive to seafloor disturbance and impacts on microbial community activity. Nitrifiers were a dominant part of the microbial community at all sites at DISCOL (about 15%), which is not the case in the deeply oxygenated sediments of the CCZ (31). Nutrient recycling via nitrification was reduced in the tracks. Nitrite profiles have a narrower peak in the surface layer of the disturbed sites, indicating reduced nitrification, potentially due to the reduced amount of labile organic matter (8). While metal oxidation has been discussed as a potential source of DCF in the CCZ (24), we found no evidence for it at DEA. We did not detect a significant release of dissolved reduced metal compounds apart from Mn^{2+} diffusing into the oxic zone, where it would precipitate as MnO_2. Furthermore, we did not detect any signs of hydrothermal energy inputs (9). Significant rates of Fe(III) reduction in the surface sediments seem unlikely because NO_3^- extends several meters into the sediments at DISCOL (9). NO_3^- is consumed at this depth, oxidizing the clay-bound Fe(II) to Fe(III), which ultimately remains bound within the clay mineral crystal structure (9). A stable total iron content in the solid phase indicates that no significant mobilization of dissolved Fe_{2+} occurred during particulate organic carbon (POC) degradation. This finding is corroborated by dissolved iron concentrations remaining below detection limit (i.e., 0.5 μM). Hence, we conclude that chemoauto-lithotrophic metal oxidation likely plays no role at DISCOL; however, we cannot rule out some cryptic biogeochemical cycles (32).

Microbial activities and cell abundances are still reduced after 26 years in some microhabitats in the plough tracks, i.e., (i) subsurface patches and (ii) ridges. The removal of the bioactive sediment layer, potentially in combination with subsequent erosion, exposed sub-surface sediments in these microhabitats, leading to a reduction in microbial abundance by 30%, also after 26 years. Assuming that cell numbers were initially reduced by 50% compared with reference sediments (as observed for EBS tracks) and adopting lowest bacterial doubling times reported for abyssal depths of 200 to 700 days (33) and a deep-sea microbial biomass turnover of 5% per year (34), the recovery of microbial abundances should have occurred within 2 to 10 years. However, diagenetic and food web modeling suggest that due to removal of the reactive surface layer, biogeochemical fluxes and rates within the DEA may be repressed for hundreds of years (9, 35). This is due to the slow buildup (i.e., 20 to 30 thousand years) of fresh sediments enriched in labile organic matter (k values of 0.1 to 0.001 year^{-1}, i.e., turnover times of 10 to 1000 years). Furthermore, bioturbation activity by benthic dwellers needs to recover to mix labile POC into the sediments, thereby increasing POC degradation efficiency (8). In the Eastern Pacific, organic matter reactivity decreases sharply in the top centimeters of deep-sea sediments, and the less reactive fraction in lower layers has first-order rate constants

with as little as 0.01 year^{-1}, corresponding to a turnover time of 100 years (36).

Hence, the removal of the bioactive sediment layer apparently does not only remove most types of microbes and, consequently, microbial activity, but also causes a general loss of labile organic matter as well as the specific sediment matrix needed for growth and recovery of the community. However, the microbial community structure remained rather similar across all disturbance levels.

In this regard, we falsified our third hypothesis, namely, that microbial community structure would be a sensitive measure of seafloor disturbance. The 16S ribosomal RNA (rRNA) tag sequencing of the surface microbial communities did not detect a significant dissimilarity between microbial communities of the DEA and the reference sites (table S2). This indicates that the loss of seafloor integrity and the displacement of sediments by ploughing did not select for specific communities but had a general negative effect on microbial activity. The high spatial variability between the microbial communities found at the reference stations (turnover between 28 and 34%) makes it difficult to resolve common disturbance-related patterns. Sequencing efforts in the Clarion-Clipperton Fracture Zone (CCFZ) showed more homogenous community structures in different sediment samples with higher differences within the same core (31). However, as we did not reach a saturation level in the rarefaction curves, we cannot rule out significant differences in the rare microbial taxa, which need further assessment.

The similarity of the microbial community in the fresh EBS track and the subsurface sediments of the DEA and reference sites support the hypothesis of the exposure of subsurface sediment communities by the disturbance (Fig. 5A). In the EBS track, unique OTUs belonging to the Chloroflexi group could be identified. In earlier studies at the Peru margin, Chloroflexi have been identified as dominant bacteria in the deep subsurface of several meters sediment depth (37) and in sediments of other manganese nodule provinces (31).

All currently available mining technologies for manganese nodules would involve massive disturbance of the uppermost 10 to 15 cm of the surface sediments (38), comparable to the simulated disturbances with a plough harrow or EBS as investigated here, but happening on much larger spatial scales. Commercial deep-sea mining is expected to affect hundreds to thousands of square kilometers of seabed per year (38). The DISCOL experiment was performed in an area of 11 km^2 with less disturbed areas between the tracks (3). Hence, losses of biogeochemical functions will have to be expected on much larger spatial scales, also reducing the chance for ecosystem recovery by lateral effects (e.g., redistribution of organic matter and recolonization). We showed that the loss of the surface sediment layer will result in long-term decreased microbial activities, lower organic matter turnover, reduced nitrogen cycling, and lower microbial growth rates. The recovery would go beyond several decades because sediment accumulation rates in nodule areas are low and bottom currents are slow. As microbial communities form the very basis of the benthic food web, benthic fauna such as meiofauna and macrofauna that depend on microbial biomass production, either directly or indi-rectly, take even longer to recover (6). The extent of the mechanical disturbances will depend on the technology of nodule mining, as well as on conditions of bottom currents and sediment accumulation speeds (2). Hence, our results indicate that ecologically sustainable technologies should avoid removal of the bioactive surface layer. Mining activities are not expected to happen in the Peru Basin, but in the CCZ, where much lower productivities lead to oxygen penetrating

several meters into the sediment and even reaching the bedrock. Consequently, the recovery time is expected to take much longer, and monitoring methods have to be very sensitive in order to detect changes on shorter time scales.

This study also contributed to identifying sensitive monitoring technologies for baseline studies, initial disturbance, and recovery. These technologies can be used for efficient environmental management protecting biological diversity and ecological integrity as outlined in the draft regulations on exploitation of mineral resources by the International Seabed Authority (39). Our observations of large spatial heterogeneity of communities, biogeochemical properties, and processes indicate that a proper replication on a small spatial scale is necessary, as well as a good coverage of natural variability in baseline studies. The observation heterogeneities on a larger scale, e.g., between reference stations with respect to diversity and biogeochemical settings (Fig. 5C), also emphasize the need to have set-aside areas with similar characteristics to be able to assess natural changes and variability in undisturbed sites for comparison with disturbance effects. This is probably not the case for the Areas of Particular Environmental Interest in the CCZ that can be less productive and biologically diverse compared with the potential mining sites (40). These aspects need to be considered when selecting Impact and Preservation Reference Zones.

The quickest and more efficient measure of seafloor integrity is the direct visual assessment of the surface seafloor, as well as the sediment layering and color in the cores. The presence and thickness of the brownish, bioactive surface layer were very good indicators of overall biological activity. However, this may not be applicable in the CCZ, where the surface sediment layer is less distinct from subsurface sediments (41). CT scans appear to be particularly useful for monitoring the physical condition and integrity of sediments after disturbances. We found that rather simple measures of seafloor physical and biogeochemical conditions allowed assessing the degree of disturbance and including the loss in biological and biogeochemical functions. Differences in half of the biogeochemical parameters shown (Figs. 3 and 4) appear to be detectable with less than eight samples with relatively high confidence (power = 0.8; table S1). Total microbial cell counts were an efficient method for estimating the impacts on the microbial community, along with rapid, on-board assays of the extracellular enzymatic activity (EEA) of enzymes such as beta-glucosidase activity. In situ oxygen profiles are highly sensitive measures of respiration rates and microbial growth efficiencies; however, they need advanced and costly deep-sea in situ technologies to be operated, which are currently only available at a few institutions within the scientific community. Changes in microbial community structure were not significant, but baseline studies of the initial disturbance did not assess this parameter. Hence, retrieval and long-term storage of environmental samples from seabed areas to be explored and exploited are an imperative for ecological assessments.

MATERIALS AND METHODS
Study design
The maximum possible number of samples (due to allocated time) was triplicate sediment cores at three different locations for five microhabitats and one location for the fresh EBS track. These samples allowed enough replication on different spatial scales to test the validity of our findings. When possible, samples were measured in technical triplicates. The sampling was based on AUV and ROV footage of the seafloor, and the sample size was defined before sampling took place. AUV footages on the first leg allowed mapping of the tracks, while ROV footages allowed finding the different microhabitats. Samples outside the tracks were taken blindly with a multicorer (MUC) or lander. All data were included, except for oxygen profiles and benthic flux chamber data that had a clearly broken sensor, as well as dark carbon fixation data with outliers in technical triplicates, which could be traced back to errors in the laboratory. Outliers are shown in the boxplots of the manuscript and included in all statistical analyses. Blinding of the analyses was ensured by the use of instruments that are unbiased to previous expectations. Cell counts were done by a student who did not know the background of the samples. The aim of the study was to test for differences of different biogeochemical, sedimentological, and microbiological parameters of different disturbed microhabitats compared with reference stations outside the disturbed area.

Location and sampling
All sampling activities and in situ measurements were carried out during the SONNE cruise SO242 (28 July 2015 to 1 October 2015) in the Peru Basin in the South Pacific at 7°S and 88.5°W (fig. S1) within and around the area of the long-term DISCOL. During the original DISCOL experiment in February/March 1989 (42), a seafloor disturbance of the benthic ecosystem was simulated by recurrent towing of a plough harrow across an area of 11 km^2 at water depths between 4140 and 4160 m (3, 43).

Replicate samples were taken at three sites within the DEA and at three reference sites located to the west, south, and east (fig. S1). During leg 1, samples were taken inside and outside the tracks using an MUC for porewater analyses and computer tomographic imaging. Porewater was analyzed in about 1-cm slices down to 15 to 25 cm. A fresh track was created with an EBS used to collect benthic and demersal fauna, which was used as fresh disturbance impact for sampling during leg 2, 5 weeks later. The EBS eroded surface sediments, creating an even, recessed track where subsurface sediments are exposed and piling up a ridge of sediments at the rim (Fig. 1).

During leg 2, an ROV (Kiel 6000) was used to sample morphologically different microhabitats in the old and new impact areas. Specific microhabitats were sampled: (i) ridges that were piled up during the ploughing; (ii) furrows between the ridges; (iii) subsurface patches, indicating exposed subsurface sediments in the tracks; and (iv) seafloor outside the tracks affected by resettled sediment from the suspended plume. The sampling was performed using the push core (PUC) system of the ROV Kiel 6000 or with a standard MUC. The cores were sliced at 4°C into different layers (0 to 1, 1 to 2, 2 to 3, 3 to 5, and 14 to 16 cm), which covered oxidized and reduced sediment layers. For porosity measurements, one core per microhabitat and site was processed with higher depth resolution. For all other analyses, the sediments of three PUCs or one to two MUCs were pooled and subsampled in triplicates coming from different cores. For CT scans, one core per site and microhabitat was stored as a whole at 4°C.

Sediment properties
Sediments were prepared for concentration measurements of phytopigments, organic matter, and porosity. Porewater was extracted for measurements of dissolved nitrite (NO_2^-), nitrate (NO_3^-), ammonium (NH_4^+), ferrous oxide (Fe^{2+}), and TA concentrations. The depth of the brown oxidized surface layer was measured directly on

freshly retrieved cores using a ruler. The brown layer represents an oxidized layer of high MnO_2 concentrations (8). Later, the same cores were used for the x-ray attenuation (density) determination via CT.

On board, 5 ml of sediment was sampled with a cutoff syringe for each layer (0 to 1, 1 to 2, 2 to 3, 3 to 5, and 13 to 16 cm). The syringes were sealed with caps, wrapped in aluminum foil, and stored at −20°C. The Chla and phaeopigment concentrations were measured using an acetone extraction method (44). The sediment and 8 ml of cold acetone (100%) were transferred into Greiner tubes, containing six glass beads, and shaken in a cell mill for 3 min. The samples were then centrifuged at 188g for 10 min at 0°C, and the supernatants were transferred into new 15-ml tubes. Acetone was added two more times, and the supernatant was added to the 15-ml tube each time. After a last centrifugation step of the extract for 2 min at 188g and 0°C, 1 ml of the extract was transferred into a cuvette and measured at a Turner Trilogy fluorometer at an excitation wavelength of 428 nm and an emission wavelength of 671 nm. For the phaeopigment measurement, one drop of HCl (25%) was added to the extracts, which were then remeasured.

Total particulate inorganic and organic carbon and nitrogen were measured using an elemental analyzer Fisons after freeze-drying, homogenizing, and preweighing of the samples. The samples were measured before (TC and TN) and after (TOC) acidification with HCl (removing inorganic carbon quantitatively as CO_2), and the concentration was calculated after measuring of sulfanilamide standards using the program Eager 200.

Dissolved NO_2^-, NO_3^-, NH_4^+, Fe^{2+}, and TA were measured directly on board in porewaters extracted from PUC and MUC sediments. Porewater was extracted at 4°C in a glove bag in an oxygen-free argon atmosphere using a low-pressure squeezer (applying argon at 3 to 5 bar). While squeezing, the porewater was filtered through a 0.2-µm regenerated cellulose Whatman filter and collected in a recipient vessel. Colorimetric methods as described by Grasshoff *et al.* (45), using a Hitachi ultraviolet/visible spectrophotometer (Hitachi High-Technologies Co., Tokyo, Japan), were used for the chemical analyses of the nutrients. TA was titrated with 0.02 N HCl against an indicator mixture of methyl blue and methylene red. The titration vessel was purged with argon to strip any produced CO_2 from the solution.

Porosity was determined by weight difference before and after freeze-drying of the sediments and converting to pore volume fraction as described by Haeckel *et al.* (8). The PUCs and MUCs were photographed, and the depth of the brown sediment was directly measured on board using a ruler. Sediment coring may smear the brown layer along the sides into deeper layers. Thus, the measured brown layer depth is seen as a maximum value.

One core per microhabitat was scanned by a Toshiba Aquilion 64 CT at the hospital Klinikum Bremen-Mitte with an x-ray source voltage of 120 kV and a current of 600 mA. The CT image stacks have a resolution of 0.35 mm in the *x* and *y* direction and 0.5-mm resolution in the *z* direction (0.3-mm reconstruction unit).

The analyses were performed with the Zuse Institute Berlin (ZIB) edition of the Amira software (version 2016.25). Prior to the analysis, the core liners, including about 2 mm of the core rims, were deleted from the dataset. Open and sediment-filled burrows, manganese nodules, and the matrix sediment were segmented by a combination of threshold and marker-based watershed segmentation. Thresholds and markers were optimized for each core individually. Quantification

of the phases and the respective x-ray density was achieved with the MaterialStatistics module.

In situ measurements

Oxygen uptake in the sediment was determined from in situ microsensor profiles (DOU) and benthic flux chambers (TOU) as described by Boetius and Wenzhöfer (46). In the disturbance area, the instruments were deployed with the ROV, and in the reference areas, the instruments were attached to a lander system (43). The profiler was equipped with five to eight Clark-type oxygen electrodes (47), while oxygen macrooptodes were used in the case of the benthic chambers (see below).

Oxygen microsensor profile analyses

The sediment surface was determined manually as a turning point in the slope where oxygen starts to get depleted. A diffusive boundary layer could not be determined in any of the profiles. The sensor raw currents were calibrated with a two-point calibration. The microsensor reading in the water column served as one calibration point. The corresponding oxygen concentration in the bottom water was measured after sampling with a Niskin bottle mounted on a water sampler rosette about 1 m above the seafloor using the Winkler titration (45) and was 150 ± 5 µM. The titration was carried out automatically using the Methrom Titrino titration device and the program tiamo v.2.3. The zero-oxygen reading was determined in the anoxic zone of the profiles, where oxygen reached a constant value. Only few profiles showed a constant reading at depth. Thus, zero-oxygen readings of the same sensor were used for calibrating following profiles of the same station if signal drift did not occur and the anoxic part was not reached. In cases where none of the profiles reached the anoxic part, zero readings obtained on board in seawater that had in situ temperature and was deoxygenated by sodium dithionite addition were used instead. The oxygen penetration depth was assigned as the depth below the seafloor where the dissolved oxygen concentration dropped below 5 µM.

The oxygen flux was derived by simulating each concentration-depth profile using a simplified diagenetic model (8). The model allowed the calculation of oxygen fluxes in non–steady-state conditions (EBS track) and in profiles not reaching 0 µM oxygen. Besides, resulting kinetic constants are informative for further biogeochemical analyses. The model treats organic matter in a reactive and a refractory fraction. A respective exponential function was fitted to the observed porosity (fig. S3) and TOC data (Table 1) and prescribed in the partial differential equation

$$\phi \frac{\partial O_2}{\partial t} = \frac{\partial}{\partial x}\left(\frac{\phi D_{O2}}{1 - 2\ln(\phi)} \frac{\partial O_2}{\partial x} + \phi u O_2\right) -$$

$$\phi \frac{138}{106} \frac{O_2}{K_{O2} + O_2} \frac{\rho_s}{M_{Corg}} \frac{(1 - \phi)}{\phi} \sum_{i=1}^{2} k_i \, TOC_{i0} \, e^{-a_i x}$$

where ϕ is porosity; D_{O2} is the molecular diffusion coefficient of oxygen, corrected for pressure, temperature, and salinity; u is the sediment accumulation velocity [i.e., 0.5 cm/thousand years (8)]; K_{O2} is the Monod constant for using oxygen (= 0.08 µM) in TOC degradation; ρ_s is the density of the solids (i.e., 2500 g dm^{-3}); M_{Corg} is the molar mass of carbon (i.e., 12 g mol^{-1}); k_i are the kinetic constants of the reactive ($i = 1$) and refractory ($i = 2$) TOC fractions (fig. S7); TOC_{i0} are their respective concentrations at the seafloor (Table 1); a_i are the fitting parameters for the exponential decay of TOC with depth; t is time; and x is sediment depth.

Adjustable parameters for reproducing the measured in situ O_2 profiles in the model simulations (fig. S7) are the kinetic constants k_i. The simulations were run until steady state was achieved, except for the EBS stations, where the simulated time was 5 weeks, matching the evolved time between towing the EBS and sampling. The partial differential equation was solved numerically using the "pdepe" built-in function of MATLAB (The MathWorks, edition R2012). A Dirichlet boundary condition was applied at the sediment surface (i.e., the oxygen bottom-water concentration of 150 µM) and a Neumann boundary condition (i.e., a zero gradient) at the bottom of the model domain.

Benthic flux chamber oxygen concentration time series analyses
Benthic flux chambers were deployed to quantify TOU of the seafloor as described by Boetius and Wenzhöfer (46). For lander-based deployments, rectangular polyacetal chambers (0.2 m by 0.2 m surface area, type K/MT 110, K.U.M. Umwelt und Meerestechnik, Kiel, Germany) were used, while the ROV-manipulated chamber modules were equipped with custom-built, cylindrical acrylic chambers (19 cm in diameter). The overlying water was kept mixed by stirring (stirrer type K/MT 111, K.U.M. Umwelt und Meerestechnik). The chamber volume of the lander chambers was determined from the distance of the lid to the surface of the recovered sediments. For the cylindrical ROV-deployed chambers, the volume was determined from the dilution of a neutrally buoyant 50-ml bromide tracer solution that was injected to the overlaying water at the beginning of the deployment. Bromide concentrations in samples taken during the deployment by an automated syringe sampler were determined in the home laboratory by ion chromatography. Visual assessments of water column height from ROV-HD video imagery were in good agreement with Bromide-based chamber volumes and used for volume determination for some deployments, where bromide injection or sampling failed. Oxygen concentrations in the overlying water were monitored by means of oxygen macrooptodes (type 4330, Aanderaa Data Instruments AS, Bergen, Norway). To monitor sensor drift that is typically observed in oxygen optodes in deep-sea applications, additional optodes were positioned outside the chambers in bottom waters at stable oxygen conditions. Raw readings from all optodes were corrected on the basis of two-point calibrations carried out after the expedition at in situ temperature. Sensors were immersed in (1) air-saturated water [concentration determined in triplicates by Winkler titration as described by Grasshoff et al. (45)] and (2) anoxic water with sodium dithionite added until constant sensor reading. Oxygen data were analyzed using MATLAB. To determine TOU, the oxygen decrease in the overlying water was determined by linear regression of the corrected sensor readings for the first 72 hours of the deployment, starting from the beginning of oxygen decrease (indicating the moment the chamber was inserted into the sediment). Oxygen decrease, recorded in the chambers, was corrected by the drift determined with the external optodes in the same period (i.e., apparent changes in bottom water oxygen in the first 72 hours). Oxygen fluxes were calculated from drift-corrected rates of oxygen concentration decrease times overlying water height (i.e., sediment area divided by overlying water volume).

Extracellular enzymatic activity
As a first measurement for the microbial activity and their capability of using different substrates via extracellular enzymes, the EEA was performed directly on board. Slurry of sediment and sterile filtrated seawater (1:1 ratio) was prepared, and the enzymatic activities of beta-glucosidase, chitobiase, aminopeptidase, and esterase were measured after Boetius and Lochte (26). The following substrates were used: for beta-glucosidase, beta-glucoside with the fluorochrome 4-methylumbelliferone (MUF) (100 µM final concentration); for chitobiase, N-acetyl-glucosamine with the fluorochrome MUF (100 µM final concentration); for aminopeptidase, leucine with the fluorochrome 7-amino-4-methylcoumarin (MCA) (500 µM final concentration); and for esterase, fluorescein diacetate (FDA) with the fluorochrome FDA (100 µM final concentration). The samples were processed and incubated at in situ temperature (2°C) within 1 day after sampling and immediately after subsampling of the cores. The samples were incubated on a shaker, subsampled three to five times after 0.5 to 1 hour and measured on a fluorescence spectrophotometer (Hitachi F-2700) after addition of borate buffer and filtered seawater.

Dark CO_2 fixation
For estimating the fixation rates of inorganic carbon, the $[^{14}C]$-bicarbonate method modified after Molari et al. (28) was applied. One milliliter of slurry [~1:1 mixture of sediment and sterile filtrated (0.22 µm) seawater] was incubated with 12 µl of ^{14}C-labeled sodium bicarbonate (0.25 mCi ml^{-1}; final activity, 3 µCi). The samples were incubated at in situ temperature (2° to 4°C) in the dark. After 24 hours, the incubations were stopped with 1 ml of formaldehyde in seawater (final concentration, 2%) and stored at 4°C on board. Controls were killed with 1 ml of formaldehyde in seawater before addition of the tracer. For testing for a linear uptake of dissolved inorganic carbon (DIC), a time series was performed with incubations for 6, 12, 24, 36, 48, and 72 hours.

The samples were then centrifuged at 12,000g for 5 min, and the supernatants were transferred to new 15-ml vials for measuring the ^{14}C-labelled DOC. The remaining sediment was washed three times with 1× phosphate-buffered saline containing 23 mM sodium bicarbonate. After each centrifugation step, the supernatants were saved for the DOC analysis. The pellet was then resuspended with 1 ml of 3 M HCl and transferred into a new 50-ml vial. Five hundred microliters of 3 M HCl was then used to wash and transfer the remains into the new tube. The 50-ml tube with the sediments was then mixed constantly by bubbling with pressurized air for 4 hours. Scintillation cocktail Ultima Gold (8 ml) was then added, and the mixed sample was centrifuged at 3500g for 30 min. The supernatant was transferred into a 20-ml scintillation vial, and the pellet was resuspended in 8 ml of Ultima Gold and centrifuged a second time. The supernatants were combined and measured with a liquid scintillation counter for a maximum of 10 min. The DOC solution was bubbled for 4 hours, and an aliquot of 0.5 ml was transferred into a scintillation vial with 8 ml of Ultima Gold and measured in the liquid scintillation counter. A few DOC solutions were filtered through 0.2-µm polycarbonate filters to verify the absence of particles. The filters did not show any particles with ^{14}C signature in the scintillation counter.

Microbial abundances (AODC)
The total microbial abundance was assessed using the AODC method. According to this procedure, 2 ml of sediment was fixed in 9 ml of 0.22 µm of sterile filtrated bottom water containing 4% formaldehyde on board. The samples were then stored at 4°C. Back in the laboratory, the total number of cells per milliliter of sediment was determined by using the AODC method after Boetius and Lochte (26). At least

two filters with 30 grids each were counted with dilution factors between 550 and 4000 and average counts of 22 cells per grid.

DNA analyses

For assessing the microbial community structure and diversity, DNA was extracted from three sediment replicates and then sequenced.

DNA extraction

For comparisons of the microbial communities using the 16S rRNA genes, a part of the sediment was subsampled for DNA analyses. Ten milliliters of sediment was transferred into a 15-ml falcon tube and stored at −20°C. Back at the Max Planck Institute, the DNA of these samples was extracted using the MoBio FastDNA Spin Kit for soil, following the instruction manual with the following modifications: (i) After adding the sodium phosphate buffer and the soil lysis buffer, the sample was incubated for 15 min at room temperature; (ii) after FastPrep homogenization, the sample was incubated for 10 min at 65°C; (iii) after adding the binding matrix, the sample was inverted for 4 min and left for settling for another 4 min before 550 μl of the supernatant was discarded; and (iv) the final DNA on the binding matrix was solved two times in 30 μl of Tris EDTA (TE) buffer and incubated at 55°C for 5 min before centrifugation. The DNA concentrations and the purity (ratio of the absorption at 260 nm/280 nm) were then measured using an infinite200 nanoquant (Tecan, Crailsheim, Germany).

Illumina tag sequencing

Illumina MiSeq paired-end tag sequencing (read length, 2 × 300 base pairs) was performed at CeBiTec (Bielefeld) using the bacterial primers S-D-Bact-0341-b-S-17 (5′-CCTACGGGNGGCWGCAG-3′) and S-D-Bact-0785-a-A-21 (5′-GACTACHVGGGTATCTAATCC-3′) for the V3-V4 region (48), and the archaeal primers Arch349F (5′-GYGCASCAGKCGMGAAW-3′) and Arch915R (5′-GTGCTC-CCCCGCCAATTCCT-3′) for the V4-V6 region (49). The amplicon libraries were generated according to the protocol recommended by Illumina (16S Metagenomic Sequencing Library Preparation, Part # 15044223, Rev. B) by CeBiTec in Bielefeld (Germany) in a 2 × 300-bp paired-end mode. The sequences were further processed after a pipeline modified after Hassenrück et al. (50). Primer sequences were removed from the raw sequence. The sequences were then demultiplexed, merged using pear v.0.9.5, quality clipped using anaconda v.2.1, trimmed using trimmomatic v.0.32, aligned using fastqc v.0.11.2, clustered using swarm v2.0, and classified against the SILVA SSU (release 119) reference database using the sina v.1.2.10 aligner. Sequences related to mitochondria or chloroplasts were removed. Absolute singletons were removed to reduce the impacts of sequencing errors, and only OTUs or SWARMS with more than one sequence in more than two samples were kept. This step removed about 5% of the sequences. The clustering of the community structures in nonmetric multidimensional scaling (NMDS) plots did not change after excluding the singletons (ANOSIM, $P < 0.05$). The remaining OTUs were pooled for each taxonomic level using taxpooler v.2.

Data analyses and statistics

The OTUs of the 16S rRNA sequences were processed using R v.3.1. Alpha diversity indices were calculated after repeated random subsampling of the sequences. The number of OTUs, the inverse Simpson (invS) index, and rarefaction curves were calculated. For the beta diversity, the OTU turnover was calculated using the Jaccard index on presence/absence OTUs tables.

Ordination analyses were performed using the R package vegan. NMDS using Bray-Curtis dissimilarities was used to separate the samples according to their community structure in an ordination plot. For the ordinations, relative abundances of the OTUs were used. Other ordinations using the most or least abundant (OTUs with reads of more or less than 1% of all OTUs), the differentially abundant (ALDEx2), or nitrifiers as potential key taxa, or ordinations using the Jaccard index (presence absence), PCA, and ordinations after rarefaction or center log ratio transformations showed the same pattern.

Differentially abundant OTUs were identified using the ALDEx2 (ANOVA-Like Differential Expression) package for R. The significance threshold was 0.05 using Benjamini-Hochberg–adjusted parametric and nonadjusted nonparametric P values. Power analyses were performed using the R package pwr and the function pwr.t.test with the following settings: (i) P value of 0.05; (ii) the effect size based on the measured variances and means of the reference and subsurface patch and most disturbed microhabitat, or with differences set to 25 and 50%; (iii) power of 0.8, 0.9, and 0.99%; or (iv) sample size of 9. Because of the rather small sample size of our study and not normally distributed data, the results have to be interpreted carefully. The number of unique OTUs was calculated as the number of OTUs that are only present in one of the microhabitats or sites, excluding the subsurface samples (14 to 16 cm bsf).

All statistical tests were performed using R v.3.1. For testing for differences in activities, cell numbers, pigment concentrations, and porosity between the sites, a Kruskal-Wallis test was applied in order to account for nonparametric data with heterogeneous variances not accountable for by transformations as tested by histograms, the Filchner test, and the Shappiro test. Samples with too few (<3 samples) measured replicates were excluded from the tests. P values were corrected after the false discovery rate.

For the sequence data, ANOSIM analyses with false discovery rate P value corrections were performed to test for significant differences in community structures between the microhabitats and sites. The Materials and Methods should provide sufficient information to allow replication of the results. Begin with a section titled Experimental Design describing the objectives and design of the study as well as prespecified components.

SUPPLEMENTARY MATERIALS

Supplementary material for this article is available at http://advances.sciencemag.org/cgi/content/full/6/18/eaaz5922/DC1

REFERENCES AND NOTES

1. J. R. Hein, A. Koschinsky, *Deep-Ocean Ferromanganese Crusts and Nodules* (Elsevier, 2014).
2. C. L. van Dover, J. A. Ardron, E. Escobar, M. Gianni, K. M. Gjerde, A. Jaeckel, D. O. B. Jones, L. A. Levin, H. J. Niner, L. Pendleton, C. R. Smith, T. Thiele, P. J. Turner, L. Watling, P. P. E. Weaver, Biodiversity loss from deep-sea mining. *Nat. Geosci.* **10**, 464–465 (2017).
3. H. Thiel, G. Schriever, A. Ahnert, H. Bluhm, C. Borowski, K. Vopel, The large-scale environmental impact experiment DISCOL—Reflection and foresight. *Deep Sea Res Pt. II* **48**, 3869–3882 (2001).
4. L. A. Levin, K. Mengerink, K. M. Gjerde, A. A. Rowden, C. L. van Dover, M. R. Clark, E. Ramirez-Llodra, B. Currie, C. R. Smith, K. N. Sato, N. Gallo, A. K. Sweetman, H. Lily, C. W. Armstrong, J. Brider, Defining "serious harm" to the marine environment in the context of deep-seabed mining. *Mar. Policy* **74**, 245–259 (2016).
5. D. O. B. Jones, S. Kaiser, A. K. Sweetman, C. R. Smith, L. Menot, A. Vink, D. Trueblood, J. Greinert, D. S. M. Billett, P. M. Arbizu, T. Radziejewska, R. Singh, B. Ingole, T. Stratmann, E. Simon-Lledo, J. M. Durden, M. R. Clark, Biological responses to disturbance from simulated deep-sea polymetallic nodule mining. *PLOS ONE* **12**, e0171750 (2017).
6. A. Boetius, M. Haeckel, Mind the seafloor. *Science* **359**, 34–36 (2018).

7. T. Stratmann, L. Mevenkamp, A. K. Sweetman, A. Vanreusel, D. van Oevelen, Has phytodetritus processing by an abyssal soft-sediment community recovered 26 years after an experimental disturbance? *Front. Mar. Sci.* **5**, 59 (2018).

8. M. Haeckel, I. Konig, V. Reich, M. E. Weber, E. Suess, Pore water profiles and numerical modelling of biogeochemical processes in Peru Basin deep-sea sediments. *Deep-Sea Res Pt. II* **48**, 3713–3736 (2001).

9. I. König, M. Haeckel, A. Lougear, E. Suess, A. X. Trautwein, A geochemical model of the Peru Basin deep-sea floor—And the response of the system to technical impacts. *Deep Sea Res Pt. II* **48**, 3737–3756 (2001).

10. A. K. Sweetman, C. R. Smith, C. N. Shulse, B. Maillot, M. Lindh, M. J. Church, K. S. Meyer, D. van Oevelen, T. Stratmann, A. J. Gooday, Key role of bacteria in the short-term cycling of carbon at the abyssal seafloor in a low particulate organic carbon flux region of the eastern Pacific Ocean. *Limnol. Oceanogr.* **64**, 694–713 (2019).

11. A. Koschinsky, B. Gaye-Haake, C. Arndt, G. Maue, A. Spritzy, A. Winkler, P. Halbach, Experiments on the influence of sediment disturbances on the biogeochemistry of the deep-sea environment. *Deep Sea Res Pt. II* **48**, 3629–3651 (2001).

12. E. Simon-Lledo, B. J. Bett, V. A. I. Huvenne, K. Köser, T. Scoening, J. Greinert, D. O. B. Jones, Biological effects 26 years after simulated deep-sea mining. *Sci. Rep.* **9**, 8040 (2019).

13. E. Alevizos, T. Schoening, K. Koeser, M. Snellen, J. Greinert, Quantification of the fine-scale distribution of Mn-nodules: Insights from AUV multi-beam and optical imagery data fusion. *Biogeosci. Discuss.* **2018**, 1–29 (2018).

14. H. Bluhm, Re-establishment of an abyssal megabenthic community after experimental physical disturbance of the seafloor. *Deep Sea Res. Pt. II* **48**, 3841–3868 (2001).

15. H. Klein, Near-bottom currents in the deep Peru Basin, DISCOL Experimental Area. *Dtsch. Hydrogr. Z.* **45**, 31–42 (1993).

16. J. L. Reyss, N. Lemaitre, T. L. Ku, V. Marchig, J. R. Southon, D. E. Nelson, J. S. Vogel, Growth of a manganese-nodule from Peru Basin: A radiochemical anatomy. *Geochim. Cosmochim. Acta* **49**, 2401–2408 (1985).

17. M. P. Stephens, D. C. Kadko, Glacial-Holocene calcium carbonate dissolution at the central equatorial Pacific seafloor. *Paleoceanogr. Paleoclimatol.* **12**, 797–804 (1997).

18. G. T. Rowe, J. W. Deming, The role of bacteria in the turnover of organic carbon in deep-sea sediments. *J. Mar. Res.* **43**, 925–950 (1985).

19. K. Lochte, C. M. Turley, Bacteria and cyanobacteria associated with phytodetritus in the deep sea. *Nature* **333**, 67–69 (1988).

20. C. Kanzog, A. Ramette, N. V. Quéric, M. Klages, Response of benthic microbial communities to chitin enrichment: An in situ study in the deep Arctic Ocean. *Polar Biol.* **32**, 105 (2009).

21. K. Hoffmann, C. Hassenrück, V. Salman-Carvalho, M. Holtappels, C. Bienhold, Response of bacterial communities to different detritus compositions in Arctic deep-sea sediments. *Front. Microbiol.* **8**, 266 (2017).

22. A. Boetius, S. Albrecht, K. Bakker, C. Bienhold, J. Felden, M. Fernández-Méndez, S. Hendricks, C. Katlein, C. Lalande, T. Krumpen, M. Nicolaus, I. Peeken, B. Rabe, A. Rogacheva, E. Rybakova, R. Somavilla, F. Wenzhöfer; RV Polarstern ARK27-3-Shipboard Science Party, Export of algal biomass from the melting Arctic sea ice. *Science* **339**, 1430–1432 (2013).

23. R. N. Glud, J. K. Gundersen, B. B. Jørgensen, N. P. Revsbech, H. D. Schulz, Diffusive and total oxygen uptake of deep-sea sediments in the eastern South Atlantic Ocean: In situ and laboratory measurements. *Deep Sea Res. Pt. I* **41**, 1767–1788 (1994).

24. R. N. Glud, J. K. Gundersen, O. Holby, Benthic in situ respiration in the upwelling area off central Chile. *Mar. Ecol. Prog. Ser.* **186**, 9–18 (1999).

25. P. C. Griffith, D. J. Douglas, S. C. Wainright, Metabolic-activity of size-fractionated microbial plankton in estuarine, nearshore, and continental shelf waters of Georgia. *Mar. Ecol. Prog. Ser.* **59**, 263–270 (1990).

26. A. Boetius, K. Lochte, Regulation of microbial enzymatic degradation of organic-matter in deep-sea sediments. *Mar. Ecol. Prog. Ser.* **104**, 299–307 (1994).

27. A. Boetius, K. Lochte, Effect of organic enrichments on hydrolytic potentials and growth of bacteria in deep-sea sediments. *Mar. Ecol. Prog. Ser.* **140**, 239–250 (1996).

28. M. Molari, E. Manini, A. Dell'Anno, Dark inorganic carbon fixation sustains the functioning of benthic deep-sea ecosystems. *Global Biogeochem. Cy.* **27**, 212–221 (2013).

29. J. J. Middelburg, Chemoautotrophy in the ocean. *Geophys. Res. Lett.* **38**, L24604 (2011).

30. A. Das, P. P. Sujith, B. S. Mourya, S. U. Biche, P. A. LokaBharathi, Chemosynthetic activity prevails in deep-sea sediments of the Central Indian Basin. *Extremophiles* **15**, 177–189 (2011).

31. M. V. Lindh, B. M. Maillot, C. N. Shulse, A. J. Gooday, D. J. Amon, C. R. Smith, M. J. Church, From the surface to the deep-sea: Bacterial distributions across polymetallic nodule fields in the Clarion-Clipperton Zone of the Pacific Ocean. *Front. Microbiol.* **8**, 1696 (2017).

32. A. Kappler, C. Bryce, Cryptic biogeochemical cycles: Unravelling hidden redox reactions. *Environ. Microbiol.* **19**, 842–846 (2017).

33. J. L. Dixon, C. M. Turley, Measuring bacterial production in deep-sea sediments using 3H-thymidine incorporation: Ecological significance. *Microb. Ecol.* **42**, 549–561 (2001).

34. B. B. Jørgensen, A. Boetius, Feast and famine — Microbial life in the deep-sea bed. *Nat. Rev. Microbiol.* **5**, 770–781 (2007).

35. T. Stratmann, L. Lins, A. Purser, Y. Marcon, C. F. Rodrigues, A. Ravara, M. R. Cunha, E. Simon-Lledó, D. O. B. Jones, A. K. Sweetman, K. Köser, D. van Oevelen, Abyssal plain faunal carbon flows remain depressed 26 years after a simulated deep-sea mining disturbance. *Biogeosciences* **15**, 4131–4145 (2018).

36. K. Soetaer, P. M. J. Herman, J. J. Middelburg, Dynamic response of deep-sea sediments to seasonal variations: A model. *Limnol. Oceanogr.* **41**, 1651–1668 (1996).

37. A. Blazejak, A. Schippers, High abundance of JS-1-and Chloroflexi-related Bacteria in deeply buried marine sediments revealed by quantitative, real-time PCR. *FEMS Microbiol. Ecol.* **72**, 198–207 (2010).

38. P. P. Weaver, D. S. Billett, C. L. Van Dover, in *Handbook on Marine Environment Protection* (Springer, 2018), pp. 215–245.

39. International Seabed authority, Draft regulations on exploitation of mineral resources in the Area. International Seabed authority (2019).

40. D. J. Amon, A. F. Ziegler, T. G. Dahlgren, A. G. Glover, A. Goineau, A. J. Gooday, H. Wiklund, C. R. Smith, Insights into the abundance and diversity of abyssal megafauna in a polymetallic-nodule region in the eastern Clarion-Clipperton Zone. *Sci. Rep.* **6**, 30492 (2016).

41. K. Mewes, J. M. Mogollón, A. Picard, C. Rühlemann, A. Eisenhauer, T. Kuhn, W. Ziebis, S. Kasten, Diffusive transfer of oxygen from seamount basaltic crust into overlying sediments: An example from the Clarion-Clipperton Fracture Zone. *Earth Planet. Sci. Lett.* **433**, 215–225 (2016).

42. E. Foell, H. Thiel, G. Schriever, in *Offshore Technology Conference* (Offshore Technology Conference, 1990).

43. A. Boetius, RV Sonne Fahrtbericht/Cruise Report SO242-2: JPI OCEANS Ecological Aspects of Deep-Sea Mining, DISCOL Revisited, Guayaquil—Guayaquil (Equador). Kiel: Helmholtz-Zentrum für Ozeanforschung, (2015).

44. A. Boetius, E. Damm, Benthic oxygen uptake, hydrolytic potentials and microbial biomass at the Arctic continental slope. *Deep Sea Res. Pt. I* **45**, 239–275 (1998).

45. K. Grasshoff, K. Kremling, M. Ehrhardt, Methods of seawater analysis. (John Wiley & Sons, 2009).

46. A. Boetius, F. Wenzhöfer, Spotlight on technology: In situ technologies for studying deep-sea hotspot ecosystems. *Oceanography* **22**, 177 (2009).

47. N. P. Revsbech, An oxygen microsensor with a Guard cathode. *Limnol. Oceanogr.* **34**, 474–478 (1989).

48. A. Klindworth, E. Pruesse, T. Schweer, J. Peplies, C. Quast, M. Horn, F. O. Glöckner, Evaluation of general 16S ribosomal RNA gene PCR primers for classical and next-generation sequencing-based diversity studies. *Nucleic Acids Res.* **41**, e1 (2013).

49. K. Takai, K. Horikoshi, Rapid detection and quantification of members of the archaeal community by quantitative PCR using fluorogenic probes. *Appl. Environ. Microbiol.* **66**, 5066–5072 (2000).

50. C. Hassenrück, C. Quast, J. Rapp, P. Buttigieg, Amplicon. GitHub repository (2016); https://github.com/chassenr/NGS/tree/master/AMPLICON.

Citation: T. R. Vonnahme, M. Molari, F. Janssen, F. Wenzhöfer, M. Haeckel, J. Titschack, A. Boetius, Effects of a deep-sea mining experiment on seafloor microbial communities and functions after 26 years. *Sci. Adv.* **6**, eaaz5922 (2020).

Science Advances

Effects of a deep-sea mining experiment on seafloor microbial communities and functions after 26 years

T. R. Vonnahme, M. Molari, F. Janssen, F. Wenzhöfer, M. Haeckel, J. Titschack and A. Boetius

ARTICLE TOOLS	http://advances.sciencemag.org/content/6/18/eaaz5922
SUPPLEMENTARY MATERIALS	http://advances.sciencemag.org/content/suppl/2020/04/27/6.18.eaaz5922.DC1
REFERENCES	This article cites 43 articles, 3 of which you can access for free http://advances.sciencemag.org/content/6/18/eaaz5922#BIBL
PERMISSIONS	http://www.sciencemag.org/help/reprints-and-permissions

Use of this article is subject to the Terms of Service